A NEWTON-TYPE RECONSTRUCTION ALGORITHM FOR A 434 MHZ MICROWAVE IMAGING SCANNER

A. Franchois[1], **A.G. Tijhuis**[2]

[1] *INTEC Dept., Ghent Univ., St.-Pietersnieuwstraat 41, B-9000 Gent, Belgium, ann.franchois@intec.rug.ac.be*

[2] *Electr. Eng. Fac., Eindhoven Univ. of Technology, PO Box 513, 5600 MB Eindhoven, the Netherlands, A.G.Tijhuis@tue.nl*

ABSTRACT

A 2D-TM iterative complex permittivity reconstruction algorithm is presented. A particular feature of the algorithm is that the forward model accounts for the presence of the environment, in this case a circular 434 MHz microwave imaging scanner, developed at CNRS/Supélec for biomedical imaging experiments. The particular geometry of the scanner allows to apply a computationally efficient embedding technique. The reconstruction algorithm is based on quasi-Newton optimization with approximate line searches and with the BFGS formula to update the Hessian matrix. The technique is illustrated with reconstructions of an inhomogeneous lossy dielectric cylinder from simulated data.

INTRODUCTION

In the past, quantitative microwave imaging algorithms for biomedical applications have been developed and demonstrated predominantly for the case where the object under test is surrounded with a homogeneous medium of infinite extent. For this case, it is well known that a highly efficient forward solver is obtained when the fields are computed by solving a constrast-source integral equation with a combination of the CGFFT method and a special extrapolation procedure [1],[2]. In a practical imaging situation, the surrounding environment is often more complex. We refer in this paper to the cylindrical 434 MHz scanner [3], developed at CNRS/Supélec, Gif-sur-Yvette, to conduct biomedical imaging experiments. This system consists of a water-filled metal casing with a circular cross-section in which 64 transmitting/receiving antennas are regularly spaced on a circle of slightly smaller diameter. We have developed a 2D-TM iterative reconstruction algorithm, which takes into account the influence of the metal casing. This is accomplished in a computationally efficient way by applying an embedding technique to the forward model [4]. We have implemented this adapted model into a BFGS quasi-Newton optimization scheme with approximate line searches [5],"in press"[6]. This method accumulates approximate second derivative information during the iterations. In our case, the optimization operates on a nonlinear least squares cost function, representing the error between the measured field data and the field computed for a parameterized complex permittivity distribution, possibly augmented with a regularization term. Since we use different meshes for the forward modelling and the parameter reconstruction, the ill-conditioning also can be alleviated by choosing a sufficiently coarse mesh for the latter. The technique is illustrated with complex permittivity reconstructions of an inhomogeneous lossy dielectric cylinder from simulated data.

FORMULATION OF THE PROBLEM

The configuration considered in this paper is illustrated in Fig.1. An inhomogeneous, lossy dielectric cylinder with (unknown) relative complex permittivity $\varepsilon_r(\boldsymbol{\rho})$ is surrounded with water with known complex permittivity ε_{1r} and with a perfectly conducting casing with radius b. The excitation is a time-harmonic electric line source on a circular contour $\partial\mathcal{D}_O$ with radius ρ_O. There are K antennas equally spaced on $\partial\mathcal{D}_O$. Each antenna is excited in turn and the electric field is measured on all others. Source and receiver positions will be denoted with $\boldsymbol{\rho}_S = (\rho_O, \varphi_s)$ and $\boldsymbol{\rho}_R = (\rho_O, \varphi_r)$, respectively. The field caused by a line source in $\boldsymbol{\rho}_S$ can be identified as a Green's function $G(\boldsymbol{\rho}, \boldsymbol{\rho}_S)$, for which the following contrast-source integral relation can be derived:

$$G(\boldsymbol{\rho}, \boldsymbol{\rho}_S) = \bar{G}(\boldsymbol{\rho}, \boldsymbol{\rho}_S) + k_0^2 \iint\limits_{\mathcal{D}_O} [\varepsilon_r(\boldsymbol{\rho}') - \bar{\varepsilon}_r(\boldsymbol{\rho}')]\; G(\boldsymbol{\rho}', \boldsymbol{\rho}_S)\bar{G}(\boldsymbol{\rho}, \boldsymbol{\rho}')\, dA', \tag{1}$$

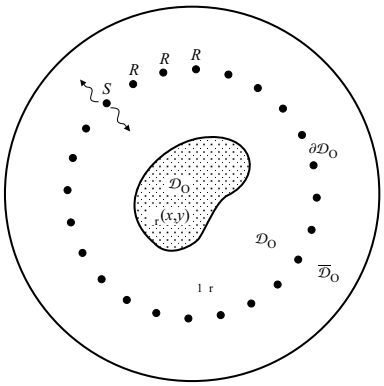

Figure 1: 2D model of the 434 MHz circular scanner configuration.

where the bars pertain to a known reference configuration, whose permittivity in $\mathcal{D}_O$ may be chosen arbitrarily. We introduce the following parameterized configuration for the unknown complex permittivity:

$$\tilde{\varepsilon}_r(\boldsymbol{\rho}) = \varepsilon_{1r} + \tilde{\chi}(\boldsymbol{\rho}) = \varepsilon_{1r} + \sum_{\alpha=1}^{N_1} \chi_\alpha \psi_\alpha(\boldsymbol{\rho}) = \varepsilon_{1r} + \sum_{p=0}^{N_{1x}} \sum_{q=0}^{N_{1y}} \chi_{p,q}\, \Lambda(x - x_p)\Lambda(y - y_q), \tag{2}$$

where $\tilde{\chi}(\boldsymbol{\rho})$ is the parameterized contrast with respect to the background medium and where the parameters $\{\chi_\alpha = \chi'_\alpha + j\chi''_\alpha\}$ are the unknowns of our problem. In (2) we assume the contrasting region to be within a computational grid consisting of $N_{1x} \times N_{1y}$ square cells with side h_1 and $N_1 = (N_{1x} + 1) \times (N_{1y} + 1)$ grid points located at $\boldsymbol{\rho}_{p,q}$. We have used two types of expansion functions $\{\psi_\alpha(\boldsymbol{\rho})\}$: bilinear functions, where $\Lambda(\xi)$ is a triangular function:

$$\Lambda(\xi) = \begin{cases} 1 - |\xi|/h_1 & \text{for } |\xi| < h_1 \\ 0 & \text{otherwise,} \end{cases} \tag{3}$$

and pulse functions, where $\Lambda(\xi)$ in (2) are replaced with:

$$\Pi(\xi) = \begin{cases} 1 & \text{for } |\xi| < h_1/2 \\ 0 & \text{otherwise.} \end{cases} \tag{4}$$

The unknowns of our problem $\{\chi_\alpha\}$ are obtained by minimizing a cost function $\mathcal{F}$ of the form

$$\mathcal{F}(\{\chi_\alpha\}) = \frac{1}{\mathcal{F}_0} \sum_{\boldsymbol{\rho}_S} \sum_{\boldsymbol{\rho}_R} |\tilde{G}^{\text{scat}}_{\text{cas}}(\boldsymbol{\rho}_R, \boldsymbol{\rho}_S) - G^{\text{scat,m}}_{\text{cas}}(\boldsymbol{\rho}_R, \boldsymbol{\rho}_S)|^2, \tag{5}$$

where $G^{\text{scat,m}}_{\text{cas}}(\boldsymbol{\rho}_R, \boldsymbol{\rho}_S)$ is the known (measured) scattered field, $\tilde{G}^{\text{scat}}_{\text{cas}}(\boldsymbol{\rho}_R, \boldsymbol{\rho}_S)$ is the corresponding field in the parameterized configuration $\{\chi_\alpha\}$ and $\mathcal{F}_0$ is a normalization constant. The subscript "scat" stands for scattered field, defined as the difference between the fields with and without the object in place. We try to alleviate the problems of local minima and ill-posedness by choosing the cell side h_1 sufficiently large. For the bilinear expansions, we also have tested the cost function (5) augmented with a regularization term [7]:

$$\delta \sum_{p=0}^{N_{1x}} \sum_{q=0}^{N_{1y}} |\chi_{p-1,q} - 2\chi_{p,q} + \chi_{p+1,q}|^2 + |\chi_{p,q-1} - 2\chi_{p,q} + \chi_{p,q+1}|^2, \tag{6}$$

where δ is a small parameter and $\chi_{i,j} = 0$ for i and/or $j < 0$, $i > N_{1x}$ and/or $j > N_{1y}$. We will denote by $\boldsymbol{\chi}$ the real vector of contrast parameters $[\chi'_1, \ldots, \chi'_{N_1}, \chi''_1, \ldots, \chi''_{N_1}]^T$, in shorthand $[\chi'_\alpha, \chi''_\alpha]^T$, in which the real and imaginary parts are ordered in the first and second half, respectively, and where ^{T} stands for transpose.

RECONSTRUCTION ALGORITHM

For the minimzation of (5) we have implemented a quasi-Newton method with linesearch [5],[6]. From iterate n to iterate $n + 1$, the contrast vector is updated with a correction $\boldsymbol{\Delta\chi}$ as follows:

$$\boldsymbol{\chi}_{n+1} = \boldsymbol{\chi}_n + \boldsymbol{\Delta\chi}_n, \tag{7}$$

$$\mathbf{p}_n = -\mathbf{H}_n^{-1}\,\mathbf{g}_n, \tag{8}$$

$$\boldsymbol{\Delta\chi}_n = \xi_n\,\mathbf{p}_n. \tag{9}$$

In (8), $\mathbf{p}$ is the Newton step, which is used as a search direction in (9). The positive real number ξ is obtained with a line search algorithm, as described in [5], such that it approximately minimizes $\mathcal{F}(\boldsymbol{\chi})$; $\mathbf{H}$ is the Hessian matrix and $\mathbf{g}$ is the gradient of the cost function

$$\mathbf{g} = 2\left[\Re\left(\frac{\partial\mathcal{F}}{\partial\chi_\alpha^*}\right), \Im\left(\frac{\partial\mathcal{F}}{\partial\chi_\alpha^*}\right)\right]^T, \tag{10}$$

where $\Re$ and $\Im$ stand for the real and imaginary parts, respectively, * is the complex conjugate and where

$$\frac{\partial\mathcal{F}}{\partial\chi_\alpha^*} = \frac{1}{\mathcal{F}_0}\sum_{\boldsymbol{\rho}_S}\sum_{\boldsymbol{\rho}_R}\frac{\partial G_{\text{cas}}^{\text{scat}\,*}(\boldsymbol{\rho}_R,\boldsymbol{\rho}_S)}{\partial\chi_\alpha^*}\left[G_{\text{cas}}^{\text{scat}}(\boldsymbol{\rho}_R,\boldsymbol{\rho}_S) - G_{\text{cas}}^{\text{scat,m}}(\boldsymbol{\rho}_R,\boldsymbol{\rho}_S)\right]. \tag{11}$$

We use the following analytic expression for $\partial G_{\text{cas}}^{\text{scat}}(\boldsymbol{\rho}_R,\boldsymbol{\rho}_S)/\partial\chi_\alpha$ [7]:

$$\frac{\partial G_{\text{cas}}^{\text{scat}}(\boldsymbol{\rho}_R,\boldsymbol{\rho}_S)}{\partial\chi_\alpha} = k_0^2\iint_{\mathcal{D}}\psi_\alpha(\boldsymbol{\rho})G_{\text{cas}}^{\text{tot}}(\boldsymbol{\rho},\boldsymbol{\rho}_R)\,G_{\text{cas}}^{\text{tot}}(\boldsymbol{\rho},\boldsymbol{\rho}_S)dA(\boldsymbol{\rho}). \tag{12}$$

In our application, computing the second derivatives $\partial^2 G_{\text{cas}}^{\text{scat}}(\boldsymbol{\rho}_R,\boldsymbol{\rho}_S)/\partial\chi_\alpha\partial\chi_\beta$, which occur in $\mathbf{H}$, is expensive and therefore avoided. We approximate this matrix based on gradient information gained in previous iterations. In particular, we use the Broyden-Fletcher-Goldfarb-Shanno (BFGS) formula for updating $\mathbf{H}^{-1}$:

$$\mathbf{H}_{BFGS,n+1}^{-1} = \mathbf{H}_n^{-1} + \left(1 + \frac{\boldsymbol{\gamma}_n^T\mathbf{H}_n^{-1}\boldsymbol{\gamma}_n}{\boldsymbol{\delta}_n^T\boldsymbol{\gamma}_n}\right)\frac{\boldsymbol{\delta}_n\boldsymbol{\delta}_n^T}{\boldsymbol{\delta}_n^T\boldsymbol{\gamma}_n} - \left(\frac{\boldsymbol{\delta}_n\boldsymbol{\gamma}_n^T\mathbf{H}_n^{-1} + \mathbf{H}_n^{-1}\boldsymbol{\gamma}_n\boldsymbol{\delta}_n^T}{\boldsymbol{\delta}_n^T\boldsymbol{\gamma}_n}\right), \tag{13}$$

where $\boldsymbol{\delta}_n = \boldsymbol{\Delta\chi}_n$ and $\boldsymbol{\gamma}_n = \mathbf{g}_{n+1} - \mathbf{g}_n$. By updating $\mathbf{H}_{BFGS}^{-1}$ we avoid to perform a matrix inversion to obtain $\mathbf{p}$ in (8). In this paper the initial search direction corresponds to the steepest descent direction.

THE FORWARD PROBLEM

The scattered field $G_{\text{cas}}^{\text{scat}}(\boldsymbol{\rho}_R,\boldsymbol{\rho}_S)$ on the measurement circle and the total field $G_{\text{cas}}^{\text{tot}}(\boldsymbol{\rho},\boldsymbol{\rho}_S)$ on the computational grid are needed to compute the cost function (5), the gradient (10) and the Hessian update in each iteration of the BFGS quasi-Newton algorithm. Applying the CGFFT method [1] combined with the marching-on-in-angle technique [2] leads to a highly efficient forward solver for the object in a homogeneous environment. The presence of the casing in our configuration breaks the convolution symmetry of the Green's function, such that operator products can no longer be evaluated with FFT operations. We therefore apply an embedding technique [4],"in press"[6], which can be implemented in a very efficient way for the circular scanner geometry. For this geometry, it is advantageous to expand the fields in terms of entire domain "outgoing" and "source-free" cylindrical wave functions. The problem at hand, which is a two-scatterers problem, involving the object and the casing, is split into two single scattering problems which are adequately coupled. The expansion coefficients of the field scattered by the casing are related to those of the fields incident on it by a diagonal matrix of reflection coefficients, which satisfy the boundary conditions of a circular perfect conductor and which are to be computed only once since the casing and water do not change during the iterations. The expansion coefficients of the field scattered by the object are related to those of the fields incident on it by a scattering matrix. This matrix is obtained by solving in each iteration the forward problem for the object in a homogeneous medium with the forementioned CGFFT method, on a grid composed of $N_{2x} \times N_{2y}$ cells with side $h_2 < h_1$. The field on the measurement circle is then obtained after solving a linear system for the unknown expansion coefficients. Finally, the induced currents on the casing are replaced by equivalent current sources on the measurement circle, yielding an elegant expression for the total field in the object in terms of the homogeneous medium solutions.

NUMERICAL RESULTS

We show reconstructions for an inhomogeneous lossy dielectric circular cylinder with a diameter of 17.6 cm ($\approx 2\lambda_1$) and containing a decentered circular hole with diameter 5 cm (Fig.2.a). The cylinder is centered on the axis of the scanner and immersed in (low-loss) water with permittivity $\varepsilon_{1r} = 76.3 - j0.1$. The relative permittivity of the cylinder is $\varepsilon_r = 65 - j2$ and the relative permittivity of the hole is equal to that of the surrounding water. The number of sources/receivers is $K = 64$. The simulated scattered field data were generated by using a fine mesh of 256×256 cells and they are free

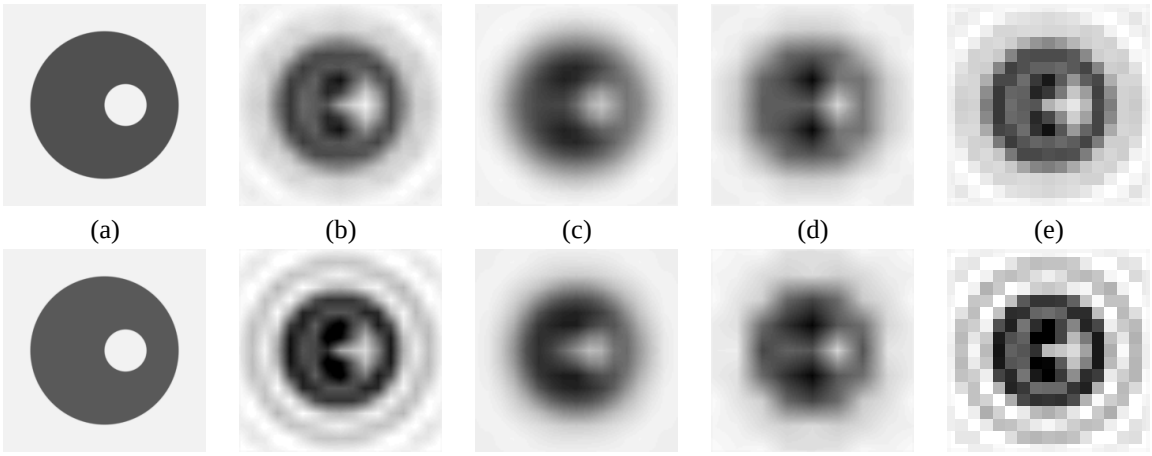

Figure 2: Real (upper) and imaginary part (lower) of the contrast: (a) exact; (b) after 40 iterations with bilinear expansion functions on a 16×16 grid; (c) after 50 iterations with regularization, (d) after 30 iterations with bilinear expansion functions on a 8×8 grid ; (e) after 40 iterations with pulse expansion functions on a 16×16 grid.

of measurement noise. For the reconstruction, we have chosen a square computational domain with side 24 cm. We parameterized the contrast on a grids of 16×16 and of 8×8 cells. For the forward-problem solution, this grid was further subdivided to 128×128 cells. The initial contrast was chosen equal to zero. In Fig.2.b, a reconstruction is shown after 40 iterations using bilinear expansion functions on a grid of 16×16 cells. In Fig.2.c we repeated this reconstruction with regularization (6), with $\delta = 10^{-6}$, yielding a smoothed reconstruction. In Fig.2.d, a reconstruction is shown after 30 iterations using bilinear expansion functions on a grid of 8×8 cells. The use of larger cells leads to less oscillations in the reconstruction. In Fig.2.e, a reconstruction is shown after 40 iterations using pulse expansion functions on a grid of 16×16 cells with side 1.5 cm ($\approx \lambda_1/5$), yielding images comparable to those of Fig.2.b.

CONCLUSION

A quasi-Newton microwave reconstruction algorithm, which takes into account the presence of the scanner environment in a computationally efficient way, has been implemented. Satisfactory reconstruction results have been obtained for an inhomogeneous lossy dielectric cylinder.

REFERENCES

[1] Z.Q. Peng and A.G. Tijhuis, "Transient scattering by a lossy dielectric cylinder: marching-on-in-frequency approach," *J. Electrom. Waves Applic.*, vol. 7, pp. 739–763, 1993.

[2] A.G. Tijhuis, K. Belkebir, P. Zwamborn, and A. Rubio Bretones, "Marching on in anything: solving electromagnetic field equations with a varying parameter," *Proceedings of the International Conference on Electromagnetics in Advanced Applications*, pp. 175–178, Torino, Italy, 1997.

[3] J.M. Geffrin, *Imagerie microonde : Etude d'un scanner à 434 MHz pour applications biomédicales*, Ph.D. Thesis of the University of Paris XI, January 1995.

[4] A.G. Tijhuis, A. Franchois, W.H.A.B. Janssen and A.P.M. Zwamborn, "Two-dimensional inverse profiling in a complex environment," *Proceedings of the Microwave Imaging Methods and Techniques Workshop, European Microwave Week*, Paris, Oct. 2, 2000.

[5] R. Fletcher, *Practical Methods of Optimization*, 2^{nd} edition, Chichester: Wiley, 1990.

[6] A. Franchois and A.G. Tijhuis, "A Quasi-Newton reconstruction algorithm for a complex microwave imaging scanner environment," *Radio Science*, accepted for publication.

[7] A.G. Tijhuis, K. Belkebir, A.C.S. Litman, and B.P. de Hon, Theoretical and computational aspects of two-dimensional inverse profiling, *IEEE Trans. Geoscience Remote Sensing*, Vol. 39, pp. 1316–1330, 2001.